RESEARCH ARTICLE
doi: 10.2306/scienceasia1513-1874.2026.014

ScienceAsia 52 (1): 2026: ID 2026014: **1–10**

Methylene blue removal from aqueous solutions using corn cobs (*Zea mays* L.)-derived graphene oxide immobilized in a chitosan/ZnO nanocomposite

Henry F. Aritonang[a,*], **Audy D. Wuntu**[a], **Widya A. Lolo**[b]

[a] Department of Chemistry, Jl. Kampus Unsrat Kleak, Sam Ratulangi University, Manado 95115 Indonesia
[b] Department of Pharmacy, Jl. Kampus Unsrat Kleak, Sam Ratulangi University, Manado 95115 Indonesia

[*]Corresponding author, e-mail: henryaritonang@unsrat.ac.id

Received 7 Jul 2025, Accepted 6 Feb 2026
Available online

ABSTRACT: Synthetic dyes are highly dangerous if not managed properly. Many studies have reported the use of economical materials and methods. In this study, GO/CS/ZnO composites were synthesized by immobilizing graphene oxide (GO) into chitosan (CS)/ZnO. The steps carried out were corncob carbonization, graphite formation, GO preparation, and finally, GO/CS/ZnO composite synthesis. The composites were evaluated as adsorbents for the methylene blue (MB) dye. The final yield achieved during the composite synthesis stage was 96.9%. This figure represents a significantly higher product recovery than that obtained in the preceding synthesis steps for both the graphite and the GO. XRD and FTIR data supported the presence of components in the composite material, as confirmed by EDS analysis, which showed elemental compositions of 55.8%, 10.9%, and 32.4% for C, O, and Zn, respectively. The morphology of each material was different; GO showed a smoother surface compared to other materials, while the composite showed agglomeration due to the combination of GO, CS, and ZnO. The adsorption activity test showed that the composite had better adsorption efficiency compared to its raw materials, with efficiencies of 89.2%, 96.6%, and 98.0% for contact time, pH, and MB concentration, respectively. The adsorption equilibrium model of the composite followed the Freundlich model. Therefore, this composite holds great promise for development as an adsorbent for synthetic dyes or other substances.

KEYWORDS: corn cobs, dyes, heavy metals, adsorption method, GO/CS/ZnO composite

INTRODUCTION

Clean and healthy water free from contaminants is crucial for sustaining life. However, the world's freshwater reserves are diminishing, and stricter regulations on permissible contaminant levels are creating challenges in meeting human needs. Many human activities consume significant amounts of clean water, which is later discharged as wastewater containing various pollutants. Dyes, which are xenobiotic and natural compounds, add color to substances. The release of colored wastewater poses significant public health and environmental concerns [1, 2]. Most dyes, both soluble and insoluble, are extensively used and produced across various industries, including paper, dyeing, pulp, textiles, paint, and leather tanning. Dyes are considered pollutants due to the coloration they impart to water and their chemical toxicity, which is deemed unacceptable. If not properly managed, these dyes can persist in the environment for extended periods, causing significant health impacts [3]. Most synthetic dyes are carcinogenic and mutagenic to various microbial species and are also teratogenic. This can adversely affect the photosynthetic activity of aquatic organisms by reducing light penetration. Furthermore, exposure to these dyes can lead to severe side effects in humans, such as kidney and liver failure [4]. Methylene blue (MB) is one of the most widely consumed dyes in the industry, used for coloring silk, wool, cotton, and paper. MB is toxic, carcinogenic, and non-biodegradable and poses a severe threat to human health, in addition to its detrimental environmental impacts. This substance also causes nausea, diarrhea, vomiting, cyanosis, shock, gastritis, jaundice, methemoglobinemia, tissue necrosis, and an increased heart rate, ultimately leading to premature cell death in tissues as well as skin and eye irritation [5].

Adsorptive removal is the most widely used method for treating various dyes due to its simplicity, operational efficiency, and suitability for low-cost applications [6]. Chitosan (CS) is regarded as a potential adsorbent material for the removal of toxic pollutants due to its amino and hydroxyl groups, physicochemical properties such as chemical stability, high reactivity, and selectivity toward pollutants, as well as its excellent chelating behavior. Additionally, CS is non-toxic, biodegradable, and characterized by low production costs [7]. CS is a natural polyaminosaccharide derived from the deacetylation of chitin, a polysaccharide primarily composed of unbranched β-(1 → 4)-2-acetamido-2-deoxy-D-glucose chains [8]. CS derivatives have been extensively studied as adsorbents to improve their adsorption capabilities. Recently, CS composites, such as CS/graphene oxide (GO), have been developed for the adsorption of heavy metals and dyes from wastewater [9] and radionuclides [10],

CS/ZnO [11], CS/magnetite [12], CS/hydroxyapatite [13, 14], CS/cellulose [15], and others. To improve the adsorption capacity of chitosan composites, Manzoor et al [16] synthesized a GO/ZnO/CS nanocomposite for the removal of Pb and Cr ions from aqueous solutions. Meanwhile, Sanmugam et al [17] reported that the CS/ZnO/GO composite exhibits antibacterial effects and better dye adsorption.

In this study, GO was synthesized from "Manado Yellow" corn cobs sourced from Indonesia and immobilized within the CS/ZnO nanocomposite. To the best of our knowledge, there are still limited published reports on the adsorption of synthetic MB dye using a GO/CS/ZnO nanocomposite. In North Sulawesi Province, Indonesia, corn is commonly referred to as "Manado Yellow" corn. This study aimed to synthesize GO/CS/ZnO nanocomposites as adsorbents for the removal of MB.

MATERIALS AND METHODS

Chemicals and reagents

The chemicals used in this study were provided by Merck (Singapore) without further purification. Corn cobs (*Zea mays* L.) "Manado Kuning" were obtained from corn farmers in Tatelu Village, North Minahasa Regency, North Sulawesi Province, Indonesia.

Preparation and production of "Manado Yellow" corn cob charcoal (CCC)

The "Manado Yellow" corn cobs (CC) obtained from the farmers were cleaned with running water and dried in an oven at 80 °C overnight. Next, they were crushed and dried in an oven at 100 °C for 3 h. After drying, the CC was ground using an herbal grinder (Model: FCT-Z100, Jakarta, Indonesia) and sieved through a 200-mesh sieve. The processed CC was heated in a furnace at 600 °C for 3 h to produce CCC.

Synthesis of graphite

The resulting CCC material was initially dispersed in a beaker containing 500 ml of distilled water and stirred at 500 rpm for 2 h. Subsequently, 70 ml of 0.26 M $FeCl_3 \cdot 6H_2O$ solution was introduced. The mixture was then agitated at a speed of 700 rpm for 24 h at ambient temperature. Following the stirring process, the mixture was dried in an oven overnight at 70 °C. The resulting dry material underwent pyrolysis at 600 °C for 2 h under a constant nitrogen (N_2) flow (0.1 l/min), using a heating rate of 10 °C/min. Once cooled, the resultant product was slowly treated with a 1 M HCl solution until the pH stabilized at approximately ~ 2, during which time the mixture was continuously stirred for 20 min. The solution was then centrifuged to separate the supernatant from the graphite precipitate. The precipitate was thoroughly washed with a distilled water-methanol mixture until the pH reached 7. Finally, the product was dried sequentially: first in an oven at 50 °C for one night, and then at 100 °C for a second night [18].

Synthesis of graphene oxide (GO)

A total of 5 g of graphite was added to a container containing 30 ml of a mixture of 24 ml H_2SO_4 (97%) and 6 ml H_3PO_4 (85%) (4:1, v/v), followed by the addition of 2 g of the oxidant $KMnO_4$. The solution was then stirred at 50 °C for 60 min, and 2 ml of a 30% H_2O_2 solution was added to stop the reaction. The solution was centrifuged, and the residue was washed with 30 ml of 30% HCl, 30 ml of absolute ethanol, and distilled water until the pH reached 7. The resulting solid GO was dried in an oven at 60 °C overnight [19].

Synthesis of GO/CS/ZnO composite

The prepared GO was added to a 2% (w/v) CS solution in 2% acetic acid solvent. This solution was then gradually dropped into 50 ml of a 0.13 M $Zn(NO_3)_2 \cdot 6H_2O$ solution. Subsequently, 5 ml of glutaraldehyde was added while stirring at 900 rpm for 5 h. Glutaraldehyde was employed as the cross-linking agent for chitosan [20]. The mixture was then heated to 60 °C, and a 0.2 M NaOH solution was gradually added until the pH reached 11, forming a white precipitate. The precipitate was collected by centrifugation for 20 min, washed three times with an absolute ethanol-water mixture to remove impurities, and dried in an oven at 50 °C for 24 h.

Characterization and measurements

The materials produced in this study were characterized using X-ray diffraction (XRD) to examine the structural properties of the samples on a diffractometer (PANanalytical, Type X'Pert PRO, Cambridge, Massachusetts). Furthermore, the structural transformation of the samples was analyzed using Fourier Transform Infrared Spectroscopy (FT-IR) with an FT-IR spectrophotometer (Shimadzu, Type IR Prestige 21, Tokyo, Japan). The morphology of the samples was characterized using a scanning electron microscope (SEM) equipped with energy-dispersive spectroscopy (EDS) (FEI, Type Inspect-S50, Hillsboro, USA).

Adsorption of MB

The adsorption study of MB on the composite began with determining the maximum wavelength of MB within the range of 400–700 nm using an MB concentration of 5 ppm. Subsequently, a standard curve was created with varying MB concentrations of 0, 0.5, 1.0, 1.5, 2.0, 2.5, and 3.0 ppm. From this standard curve, the linear regression equation $y = ax + b$ was obtained. Based on the obtained curve, the equation of the straight line can be determined and subsequently used to calculate the maximum adsorption capacity at various contact times (0, 30, 60, 90, and 120 min), pH levels (4, 7, 10), and MB solution concentrations (25, 50, 75, and 100 ppm). Each experiment was

performed with three replicates. The adsorption capacity at each contact time, pH, and MB concentration is calculated using Eq. (1):

$$\text{adsorption (\%)} = \frac{C_0 - C_e}{C_e} \times 100\% \quad (1)$$

where C_0 is the concentration before adsorption, and C_e is the concentration after adsorption.

The relationship between the amount of adsorbate adsorbed and the concentration of adsorbate in solution at equilibrium and constant temperature can be expressed using adsorption isotherms, namely Langmuir and the Freundlich. The Langmuir isotherm describes the relationship between C_e and C_e/q_e, where Ce is the final concentration, and Ce/qe is the final concentration divided by the amount of adsorbed substance, as shown in Eq. (2) [21].

$$\frac{C_e}{q_e} = \frac{C_e}{q_m} + \frac{1}{K_L q_m} \quad (2)$$

where C_e is the concentration at equilibrium (mg/l), q_e is the uptake capacity at equilibrium (mg/g), q_m refers to the maximum uptake capacity (mg/g), and K_L is the Langmuir constant (l/mg).

Meanwhile, the Freundlich isotherm represents the relationship between $\ln C_e$ and $\ln q_e$, as presented in Eq. (3) [21].

$$\ln q_e = \ln K_F + \frac{1}{n} \ln C_e \quad (3)$$

RESULTS AND DISCUSSION

Characterization of the composite

The carbonization process of CC produced a black powder, resulting from the decomposition of organic compounds like cellulose, hemicellulose, and lignin. This process also generated water vapor, methanol, acetic acid vapors, and hydrocarbons [22]. Additionally, this process aimed to remove the water content or materials not needed by the carbon. Zhao et al [23] stated that the carbonization temperature can affect the moisture content of the material. The higher the carbonization temperature, the lower the moisture content of the resulting carbon. The research results showed that the yield of CCC was 19.9%. Fig. 1 shows the carbonization results of the CC powder to CCC.

The production yield of biochar is primarily affected by two factors: temperature and the duration of the pyrolysis process. An increase in temperature leads to decreased yield, attributed to processes such as aromatization, dehydrogenation, decarboxylation, deoxygenation, and dehydration that occur at elevated temperatures, thereby enhancing carbonization. Likewise, extending the pyrolysis duration promotes the volatilization of volatile compounds, which also contributes to a reduction in yield [24]. The carbonized

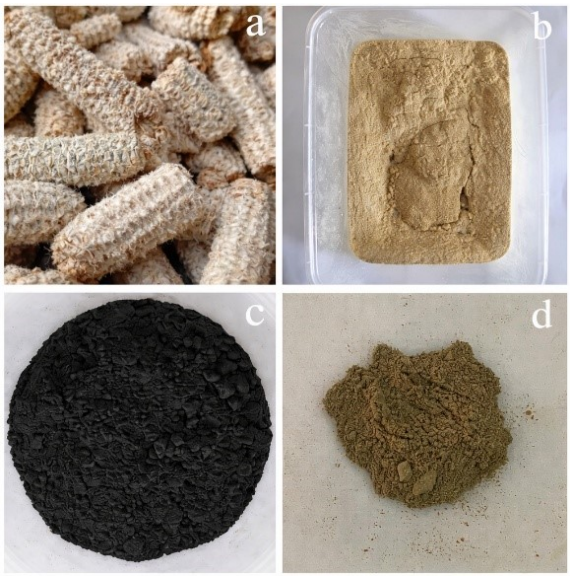

Fig. 1 Preparation of composite: (a) dried CC, (b) CC powder after crushing and sieving to 200 mesh, (c) CCC, and (d) GO/CS/ZnO.

CCC was used to synthesize graphite from CC (referred to as graphite). The results showed that the color of the graphite and GO was not significantly different from that of the carbonized CC, appearing as black powder. However, the resulting GO/CS/ZnO composite powder was brown, as shown in Fig. 1(d). The average yields of the graphite, GO, and composite were 84.2%, 89.0%, and 96.9%, respectively.

The physical differences in the research samples were also analyzed using XRD characterization, as shown in Fig. 2.

The diffractogram of each sample shows that the CC, CCC, graphite, and GO are similar, exhibiting two main peaks at 2θ values of 24.8° and 43.8°, corresponding to the reflection from (002) and (100). Generally, carbon samples show two primary peak regions at 2θ values of 24.8° and 43.8° [25]. Strong peaks were observed at 2θ = 26.1°, 28.1°, and 29.5°, indicating the presence of graphite. A high peak at 2θ = 24.0° is representative of carbon (C12 to C60) [26]. These 2θ values are also comparable to the standard carbon according to the Inorganic Crystal Structure Database (ICSD) no. 31170. However, a distinct pattern is observed in the GO/CS/ZnO composite sample, which shows seven peaks at 2θ values of 12.9°, 22.1°, 28.1°, 31.0°, 32.9°, 35.5°, and 59.6°. Upon examining the peaks of the composite, it can be concluded that the two peaks for carbon shift in the 2θ region are due to the presence of other materials besides carbon, namely chitosan and ZnO. The diffractogram displays the main peaks of chitosan at 12.9° and 21.6° [27]. These peaks are still observed, although a shift in the 2θ region is

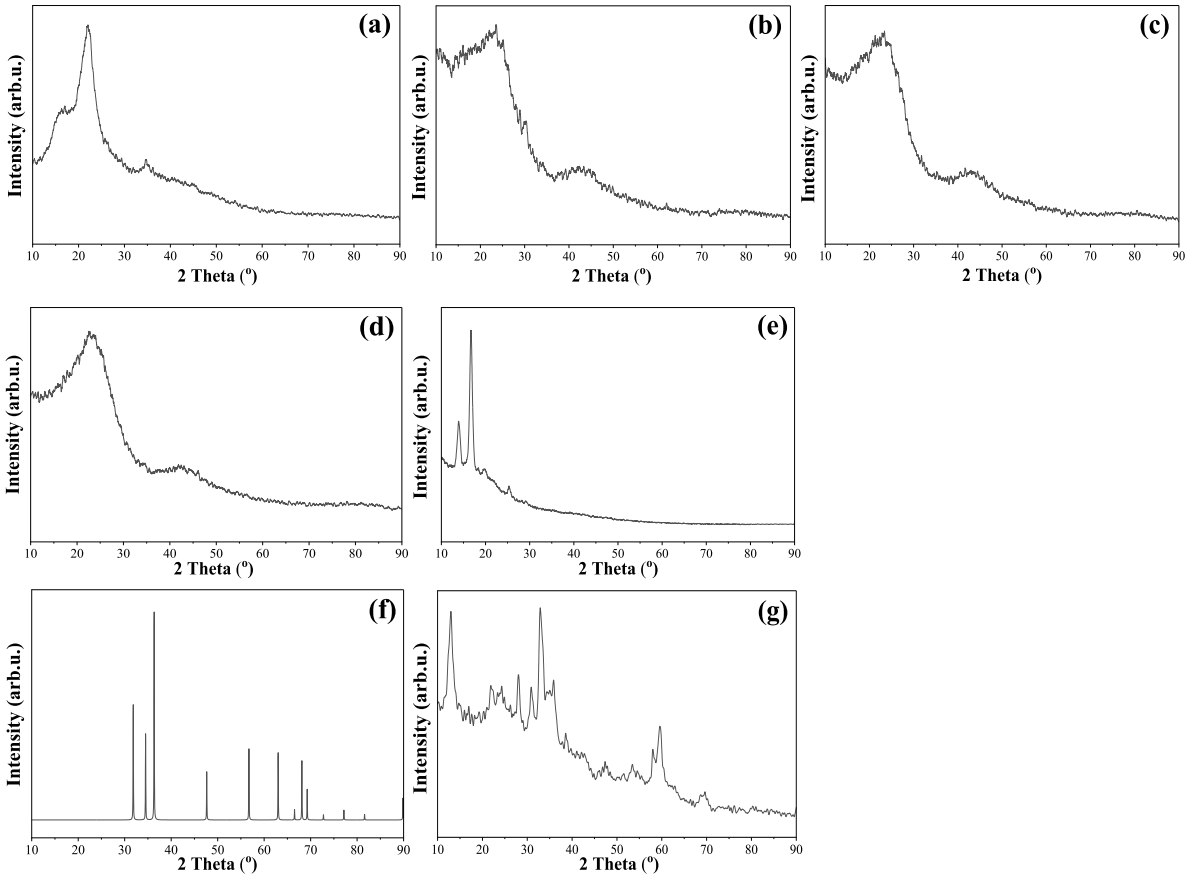

Fig. 2 Diffractogram of (a) CC, (b) CCC, (c) graphite, (d) GO, (e) CS, (f) ZnO, and (g) GO/CS/ZnO.

evident, indicating the successful grafting of CS onto the GO nanomaterials. Meanwhile, the peaks observed at 2θ values of 31.9°, 34.5°, 36.8°, 47.5°, 58.9°, 62.7°, and 69.2°, correspond to the reflection from (100), (002), (101), (102), (110), (103), (112) crystal planes of the hexagonal wurtzite ZnO structure [16]. Based on the diffraction pattern of each sample, the Full Width at Half Maximum (FWHM) data were obtained, which can be used to calculate the crystallite size of the samples. The crystallite sizes for each sample are 1.36 nm, 0.4 nm, 0.4 nm, 0.4 nm, and 1.4 nm for the CC, CCC, graphite, GO, and GO/CS/ZnO samples, respectively.

The functional groups present in the GO/CS/ZnO composite can be identified through characterization with FTIR, and the results are shown in Fig. 3. The spectrum illustrates the synthesized material as transmittance (%) versus wavenumber (cm^{-1}). The FTIR spectra indicate that the profiles of the carbon, graphite, and GO samples are relatively similar, with a broad peak observed in the wavenumber range of 3500–1700 cm^{-1}. The characteristic spectra of CS, GO, and ZnO can be detected in the FTIR spectrum of the GO/CS/ZnO aerogel, with variations in intensity and a shift toward higher wavenumbers due to the interaction between the CS polymer, GO, and ZnO.

The FTIR spectrum also shows that GO exhibits characteristic peaks, namely at 3307 cm^{-1}, indicating O—H deformation; 1726 cm^{-1}, corresponding to C=O bonds; 1583 cm^{-1}, corresponding to C=C bonds; and 1456 $cm^{-1}$and 1051 cm^{-1}, indicating the presence of C—O groups [28, 29]. Several researchers have reported that the CS spectrum shows peaks at 3294 cm^{-1} (O—H deformation), 1715 cm^{-1}, indicating the presence of C=O bonds, 1554 cm^{-1}, corresponding to N-H bending in the amide group, and 1460 $cm^{-1}$and 1030 cm^{-1} corresponding to C—O bonds [30]. The GO-CS spectrum shows peaks at 3350 cm^{-1} (O—H distortion) and 1656 cm^{-1}, as well as overlapping bands attributed to the amine groups of CS and carboxyl groups of GO at 1375 cm^{-1} and 1153 cm^{-1}, indicating C—O bonds. In addition, the characteristic signal of the secondary amide group (N—H bending) shifts to 1581 cm^{-1} (between the CS and GO-CS signals) and may overlap with other bands in the spectrum.

The main characteristic bands of ZnO nanoparticles at 1539, 1432, 1003, and 782 cm^{-1} [31] may also overlap with other bands. Furthermore, peaks ap-

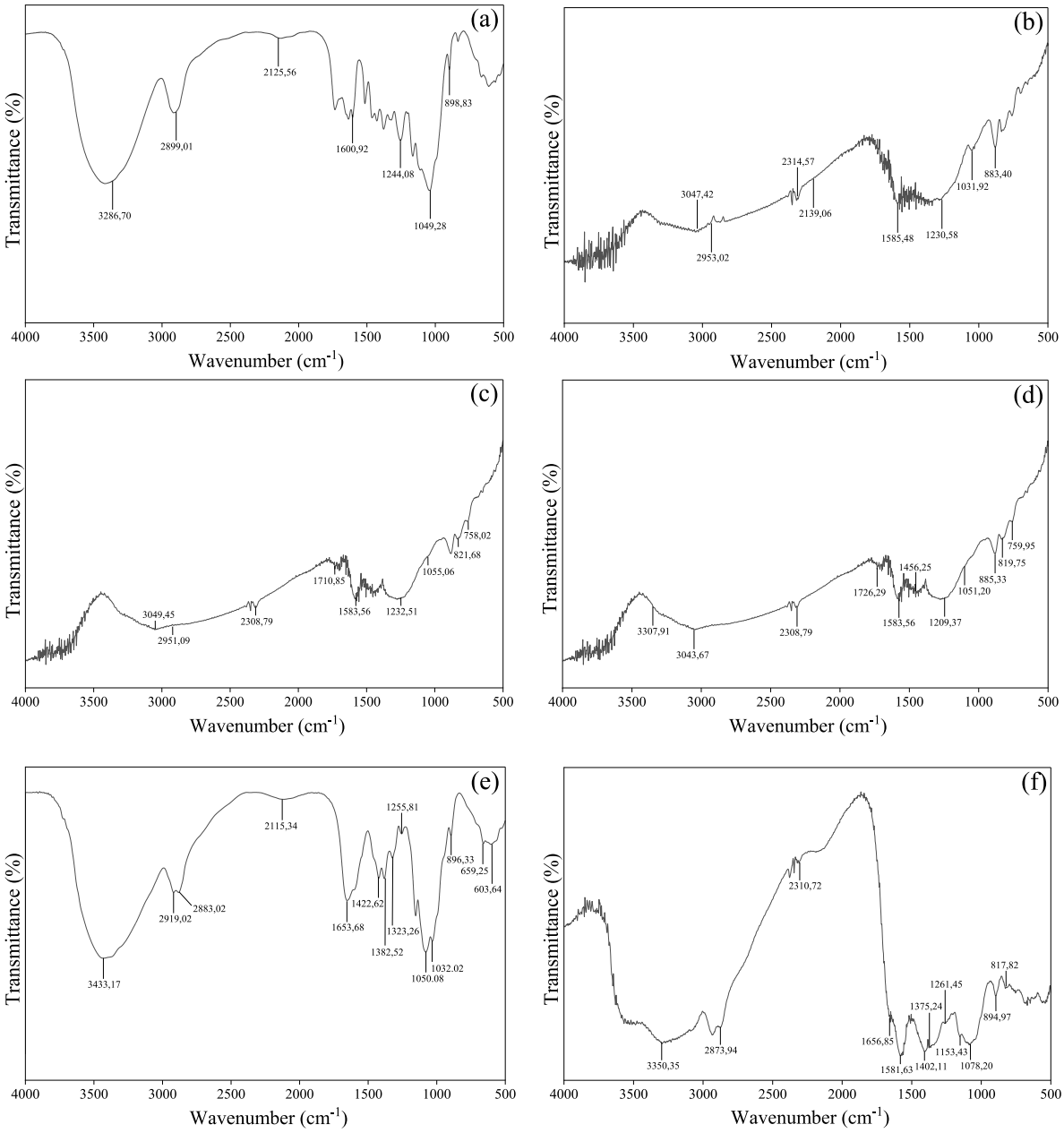

Fig. 3 FTIR spectra of the samples (a) CC, (b) CCC, (c) graphite, (d) GO, (e) CS, and (f) GO/CS/ZnO.

pearing below 1000 cm^{-1} (Fig. 3f) are attributable to interatomic vibrations of ZnO. The presence of a peak at 605 cm^{-1} indicates the bonding and modification of GO with ZnO, as evidenced by the shift of the ZnO peak from 620 cm^{-1} in the pure ZnO spectrum (Fig. 3c) to 605 cm^{-1} in the GO-ZnO nanocomposite [16]. Additionally, the bands observed at 540, 580, and 670 cm^{-1} are associated with the stretching vibrations of Zn–O nanoparticles [32]. Moreover, the broader peak at 3262 cm^{-1}, associated with the stretching vibration of NH2 and OH groups, shifts to a lower value, indicating and confirming the chemical interaction between ZnO molecules and the CS binding sites [33].

The difference in the FTIR spectrum profiles is also reflected in the variation in the surface morphology of the synthesized samples, as shown in Fig. 4.

To confirm the presence of elements from each component of the composite, an EDX analysis was conducted. The results revealed that only the CC and CCC samples exhibit the same types of elements, although their elemental percentages differ. In general, the main elements present in the CC, CCC, graphite, and GO

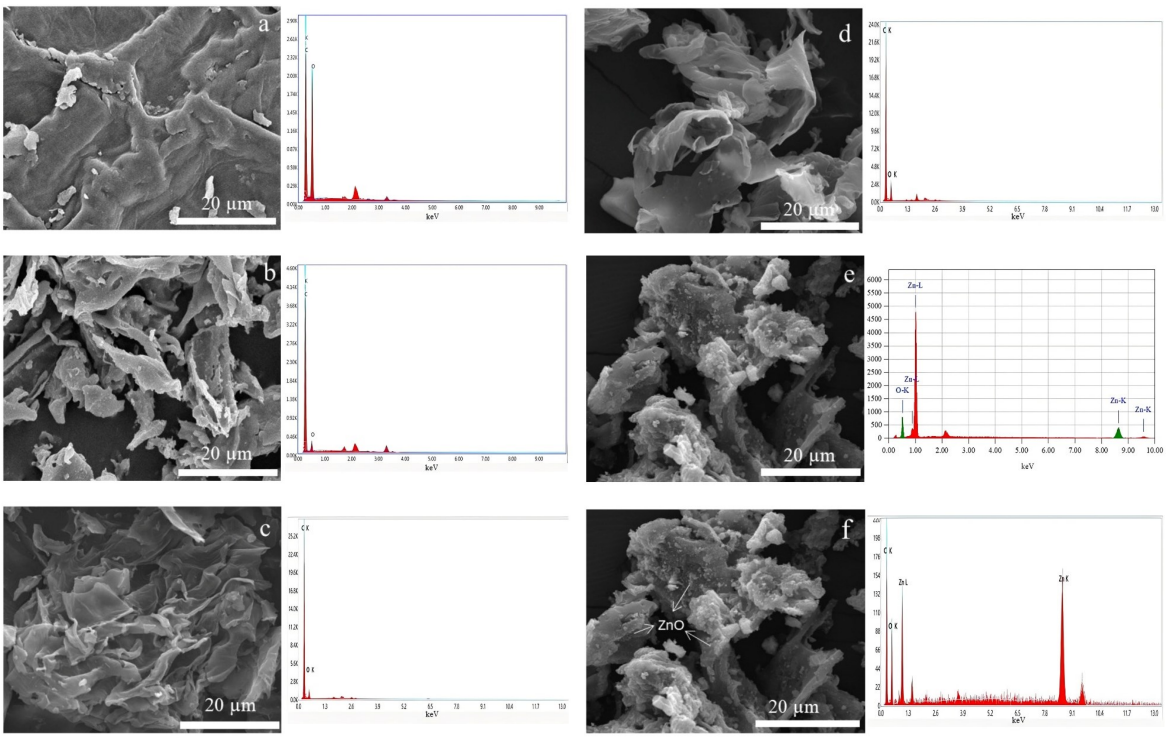

Fig. 4 SEM images and EDX graphs of (a) CC, (b) CCC, (c) graphite, (d) GO, (e) ZnO, and (f) GO/CS/ZnO.

samples are carbon (C) and oxygen (O). In contrast, the GO/CS/ZnO composite is mainly composed of carbon, oxygen, and zinc, as shown in the EDX graph. Elemental analysis of the GO/CS/ZnO composite showed a composition of approximately 55.8% carbon, 10.9% oxygen, and 32.4% zinc by weight. When expressed in atomic percentage, the composition is approximately 79.3% carbon, 11.7% oxygen, and 8.5% zinc. These findings confirm that the constituent materials were successfully integrated into the GO/CS/ZnO composite.

Adsorption study of MB

Several adsorption experiments were conducted to investigate the effects of contact time, pH, and adsorbent dosage on MB removal on the surface of GO/CS/ZnO. All experiments were carried out at room temperature. The effect of contact time was studied by varying the contact time from 30 to 120 min, as shown in Fig. 5. Adsorption efficiency increased with contact time and reached equilibrium at approximately 90 min, due to the increased availability of surface binding sites. Afterward, the adsorption efficiency became constant because the surface binding sites were insufficient [34], the GO/CS/ZnO composite demonstrated an adsorption efficiency of $89.2 \pm 0.03\%$. Nonetheless, subsequent statistical analysis indicated that the 90-min contact time was not a statistically significant differentiating factor for the performance of the various adsorbent samples The highest adsorption efficiency was achieved when using the GO/CS/ZnO composite adsorbent (Fig. 5a(4)). This information suggests that the composite has relatively more binding sites due to the presence of GO, CS, and ZnO compounds, making it more efficient in adsorption. In contrast, other samples have fewer binding sites, resulting in lower adsorption efficiency.

pH is a crucial parameter in adsorption experiments because both the adsorbent and adsorbate exhibit different properties at varying solution pH values. Consequently, we performed MB adsorption on the GO/CS/ZnO surface by adjusting the solution pH to 4, 7, and 10, while keeping other parameters constant (contact time = 90 min, concentration = 25 mg/l, and solution volume = 25 ml). The pH of the MB solution was controlled using 0.1 M NaOH and 0.1 M HCl. The experimental results are shown in Fig. 5b.

Fig. 5b indicates that removal efficiency decreases at lower pH, with maximum adsorption occurring at pH 7. The GO/CS/ZnO (Fig. 5b(4)) composite exhibited the superior adsorption efficiency at $96.0 \pm 0.004\%$. However, a key finding was that the adsorption efficiencies across all adsorbent types remained statistically comparable, showing no significant variation regardless of the pH level applied. This result can be explained by the structure of MB and the surface properties of the adsorbent at different pH levels. MB is a cationic dye that exists as a

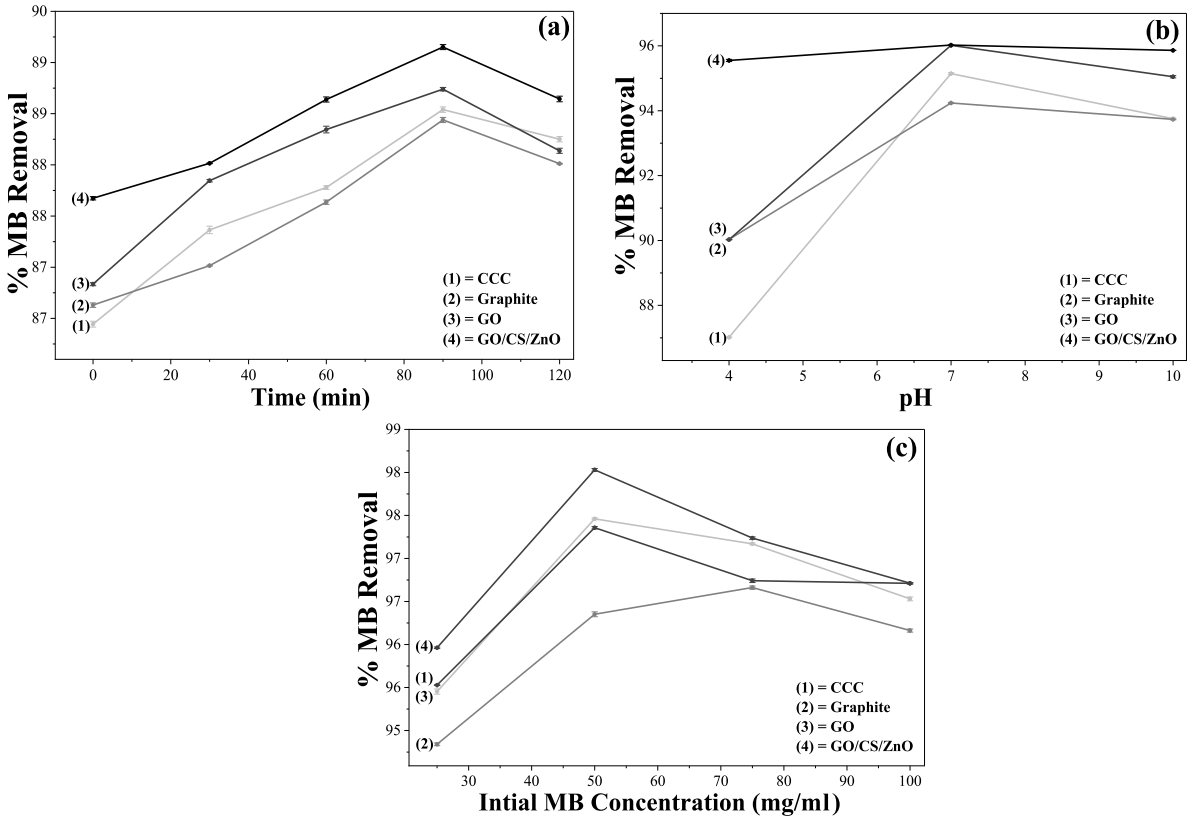

Fig. 5 The adsorption study of MB on the GO/CS/ZnO composite, (a) effect of contact time, (b) effect of pH, (c) effect of initial MB concentration.

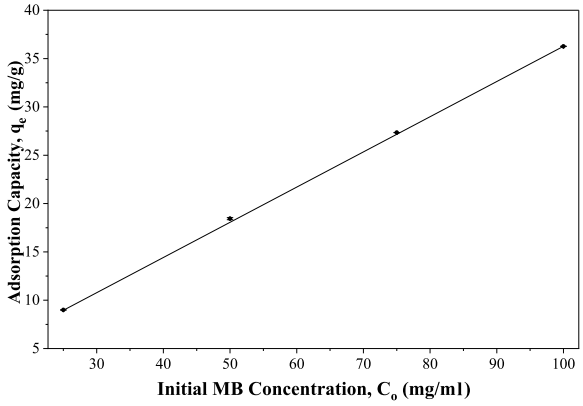

Fig. 6 Effect of initial MB concentration (mg/l) on the adsorption capacity of GO/CS/ZnO composite (mg/g).

positively charged molecule in solution [5]. Therefore, a negatively charged surface is required for effective adsorption. At higher pH levels, the surface carries more negative ions, resulting in increased MB adsorption through electrostatic interactions, whereas lower adsorption is observed at lower pH (pH 4) due to electrostatic repulsion.

Fig. 5c(4) also shows that the GO/CS/ZnO composite exhibits relatively higher adsorption efficiency compared to the other samples. It can be inferred that electrostatic interactions are not the only mechanism involved in MB adsorption; oxygen-containing functional groups also play a role in the adsorption process. These groups form hydrogen bonds and provide additional electrostatic interactions at lower pH levels, resulting in higher adsorption efficiency compared to the other samples [35]. Batch adsorption experiments were conducted to test the adsorption efficiency of MB at varying concentrations ranging from 25 to 100 mg/l while maintaining all other parameters constant: contact time of 90 min, pH 7, and adsorbent dose of 0.1 g in 25 ml of MB solution. As shown in Fig. 5c, it is evident that the adsorption efficiency increases with concentrations from 25 to 50 mg/l, except for the graphite sample, which shows an increase up to a concentration of 75 mg/l and a decrease after that. The experimental findings indicated that the GO/CS/ZnO composite exhibits optimal adsorption efficiency, achieving a maximum of $98.0 \pm 0.01\%$ at a concentration of 50 mg/l. This is attributed to the increased availability of binding sites on the adsorbent surface (the number of binding sites on the surface remains constant). At a 50 mg/l concentration,

Table 1 Parameters of Langmuir and Freundlich Isotherms for MB Adsorption.

Material	Langmuir			Freundlich		
	K_L (l/mg)	q_m (mg/g)	R^2	K_f $_{(mg/g)(l/mg)^{1/n}}$	$1/n$	R^2
CCC	1.21	29.67	0.97	8.05	1.05	0.85
Graphite	0.02	13.33	0.98	7.36	0.86	0.88
GO	0.08	107.5	0.98	14.52	2.13	0,90
GO/ZnO/CS	0.17	67.11	0.89	288.5	0.10	0.98

the adsorption efficiency of the GO/CS/ZnO composite sample was statistically comparable to all other tested samples, with the exception of the pure graphite control. Furthermore, at the higher concentration of 100 mg/l, the GO/CS/ZnO composite's efficiency remained statistically indistinguishable from the other samples, except for the CCC material. These results suggest that at the stated concentration levels, the specific type of adsorbent material does not significantly influence the overall adsorption efficiency.

Fig. 6 illustrates that the adsorption capacity of the GO/CS/ZnO composite continued to increase as the initial MB concentration rose, reaching its maximum at 100 mg/l. This positive trend can be attributed to several factors, including an increase in collision frequency [36], enhanced utilization of active surface sites [37], and a steeper concentration gradient between the liquid and solid phases. This steep gradient minimizes mass transfer resistance, thereby facilitating greater mass transport [38]. Conversely, the eventual saturation or decrease in adsorption capacity is generally attributed to a limited availability of adsorption sites [39]. Notably, the maximum adsorption capacity of the GO/CS/ZnO composite (36.3 ± 0.002 mg/g) is superior to that of an algae (*Nostoc sphaericum*)/activated clay composite (20 mg/g) [40]. However, this capacity remains lower than that reported for the sodium alginate/montmorillonite/polyethyleneimine adsorbent (148.6 mg/g) [41].

Adsorption isotherms of MB

Table 1 presents the MB absorption results correlated with the Langmuir (Eq. (2)) and the Freundlich (Eq. (3)) models. Based on the obtained R^2 data, it can be observed that the Langmuir model fits better for the CCC, graphite, and GO samples, whereas the GO/CS/ZnO sample aligns more closely with the Freundlich model. The slope value ($1/n$) reflects the adsorption intensity or surface heterogeneity. Generally, the adsorption process is considered homogeneous if the $1/n$ value falls within the range of 0.1 to 1.0 [42]. In this study, the index values for the CCC and GO samples fall within this range, indicating that the adsorption process tends to be homogeneous and proceeds effectively. Meanwhile, the index values for the graphite and GO/CS/ZnO composite samples exceed 1, suggesting that the adsorption process tends to be heterogeneous. Nevertheless, the composite's index value is relatively higher than that of graphite, indicating that the composite adsorption process is more inclined toward heterogeneity and proceeds cooperatively [43].

Nevertheless, both the CCC and GO samples exhibited a Freundlich exponent ($1/n$) greater than one, indicating an S-type isotherm. This behavior is commonly observed at low concentration ranges because both materials possess polar functional groups. At these lower concentrations, the adsorbent material directly competes with water molecules for available adsorption sites [44].

CONCLUSION

Adsorption of methylene blue by a GO/CS/ZnO composite derived from yellow Manado corn cobs was investigated. GO was successfully synthesized from the corn cobs and immobilized within the CS/ZnO matrix, forming a novel GO/CS/ZnO composite. The synthesized composite was characterized using XRD, FTIR, and SEM-EDS. The composite exhibited a maximum adsorption capacity of 67.1 mg/g for MB under optimal conditions of 90 min contact time, pH 7, and an initial MB concentration of 50 mg/l at 25 °C. The Freundlich isotherm model provided the best fit for the MB adsorption data. These findings highlight the potential of the GO/CS/ZnO composite as an effective and low-cost adsorbent for the removal of organic dyes from aqueous solutions. The composite's rapid adsorption kinetics, natural origin, and accessibility make it a promising candidate for environmental remediation applications. Finally, it has been demonstrated that GO synthesized from yellow Manado corn cobs can be immobilized into a CS/ZnO composite, resulting in a GO/CS/ZnO composite that serves as an effective and cost-efficient adsorbent for MB dye. The composite is also characterized by its rapid action, natural composition, affordability, and accessibility.

Acknowledgements: The author extends gratitude to Sam Ratulangi University for its financial support through the RDUU research scheme funded by PNBP, under contract number 636/UN12.27/LT/2024.

REFERENCES

1. Alegbe EO, Uthman TO (2024) A review of history, properties, classification, applications, and challenges of natural and synthetic dyes. *Heliyon* **10**, e33646.
2. Chaisrisongkram C, Thiwawong T, Onlaor K, Tunhoo B (2024) Preparation of calcium oxide/graphitic carbon nitrides ($CaO/g\text{-}C_3N_4$) composite for photocatalyst dye degradation. *ScienceAsia* **50**, ID 2024066.
3. Lin J, Ye W, Xie M, Seo DH, Luo J, Wan Y, Van der Brugge B (2023) Environmental impacts and remediation of dye-containing wastewater. *Nat Rev Earth Environ* **4**, 785–803.

4. Prasad S, Yadav KK, Kumar S, Gupta N, Cabral-Pinto MMS, Rezania S, Radwan N, Alam J (2023) Chromium contamination and effect on environmental health and its remediation: A sustainable approach. *J Environ Manage* **285**, 112174.
5. Khan I, Saeed K, Zekker I, Zhang B, Hendi AH, Ahmad A, Ahmad S, Zada N, et al (2022) Review on methylene blue: Its properties, uses, toxicity and photodegradation. *Water* **14**, 242.
6. Lan D, Zhu H, Zhang J, Li S, Chen Q, Wang C, Wu T, Xu M (2022) Adsorptive removal of organic dyes via porous materials for wastewater treatment in recent decades: A review on species, mechanisms, and perspectives. *Chemosphere* **293**, 133464.
7. Wang J, Zhuang S (2022) Chitosan-based materials: Preparation, modification, and application. *J Clean Prod* **355**, 131825.
8. Saheed IO, Oh WD, Suah FBM (2021) Chitosan modifications for adsorption of pollutants: A review. *J Hazard Mater* **408**, 124889.
9. Pinelli F, Nespoli T, Rossi F (2021) Graphene oxide-chitosan aerogels: synthesis, characterization, and use as adsorbent material for water contaminants. *Gels* **7**, 149.
10. Hassan RS, Sami NM, Ali MMS, Elsayed AA (2025) Adsorption performance of eco-friendly chitosan/ graphene oxide composite hydrogel for removal of ^{134}Cs and $^{152+154}$Eu radionuclides from aqueous solution. *Appl Radiat Isot* **225**, 112072.
11. Emeka EE, Onwudiwe D, Mbonu I (2021) Green synthesis, structural characterization, and photocatalytic activities of chitosan-ZnO nanocomposite. *J Inorg Organomet Polym Mater* **31**, 3356.
12. Fouda SR, Abuessawy A, Abdel-Rahman, El-Hema HS, Eisa MN, Hawata MA (2025) New functionalized magnetite chitosan-heterocyclic nanocomposites excelling in Cd^{2+} removal from aqueous solution with biological activity. *Appl Water Sci* **15**, 1–16.
13. Scalera F, Pereira SIA, Bucciarelli A, Tobaldi DM, Quarta A, Gervaso F, Castro PML, Polini A, et al (2023) Chitosan-hydroxyapatite composites made from sustainable sources: A morphology and antibacterial study. *Mater Today Sustain* **21**, 100334.
14. Rizkiana MF, Salsabila ZA, Aulia RI, Amini HW, Palupi B, Rahmawati I, Fachri BA (2024) Microwave-assisted synthesis of chitosan-hydroxyapatite composite from eggshells and its adsorption properties. *ScienceAsia* **50**, ID 2024067.
15. Ambaye TG, Vaccari M, Prasad S (2022) Preparation and applications of chitosan and cellulose composite materials. *J Environ Manage* **301**, 113850.
16. Manzoor Q, Farrukh MA, Sajid A (2024) Optimization of lead (II) and chromium (VI) adsorption using graphene oxide/ZnO/chitosan nanocomposite by response surface methodology. *Appl Surf Sci* **655**, 159544.
17. Sanmugam A, Vikraman D, Park HJ, KIM H-S (2017) One-pot, facile methodology to synthesize chitosan-ZnO-graphene oxide hybrid composites for better dye adsorption and antibacterial activity. *Nanomaterials* **7**, 363.
18. Xia S, Yang H, Lu W, Cai N, Xiao H, Chen X, Chen Y, Wang X, et al (2022) Fe-Co-based synergistic catalytic graphitization of biomass: Influence of the catalyst type and the pyrolytic temperature. *Energy* **239**(E), 122262.
19. Smith AT, Lachance AM, Zeng S, Liu B, Sun L (2019) Synthesis, properties, and applications of graphene oxide/reduced graphene oxide and their nanocomposites. *Nano Mater Sci* **1**, 31–47.
20. Barbosa RFS, Shyam S, Misra S, Mitra SK, Rosa DS (2025) Chitosan hydrogels crosslinked with glutaraldehyde for potential toxic elements removal: Batch and purification device analysis. *J Appl Polym Sci* **142**, e57539.
21. Turp SM, Turp GA, Ekinci N, Özdemir S (2020) Enhanced adsorption of methylene blue from textile wastewater by using natural and artificial zeolite. *Water Sci Technol* **82**, 513523.
22. Petrović J, Ercegović M, Simić M, Koprivica M, Dimitrijevic J, Jovanovic A, Pantic JJ (2024) Hydrothermal carbonization of waste biomass: A review of hydrochar preparation and environmental application. *Processes* **12**, 207.
23. Zhao C, Ge L, Li X, Zuo M, Chunyao X, Chen S, Li Q, Wang Y, et al (2023) Effects of the carbonization temperature and intermediate cooling mode on the properties of coal-based activated carbon. *Energy* **273**, 127177.
24. Elnour AY, Alghyamah AA, Shaikh HM, Poulose AM, Al-Zahrani SM, Anis A, Al-Wabel MI (2019) Effect of pyrolysis temperature on biochar microstructural evolution, physicochemical characteristics, and its influence on biochar/polypropylene composites. *Appl Sci* **9**, 1149.
25. Kropotin OV, Nesov SN, Polonyankin DA, Drozdova EA (2022) Structure and phase composition of electrically conductive carbon black. *J Phys Conf Ser* **2182**, 012076.
26. Hallam KR, Darnbrough JE, Paraskevoulakos C, Heard PJ, Marrow TJ, Flewitt PEJ (2021) Measurements by X-ray diffraction of the temperature dependence of lattice parameter and crystallite size for isostatically-pressed graphite. *Carbon Trends* **4**, 100071.
27. Triunfo M, Tafi E, Guarnieri A, Salvia R, Scieuzo C, Hahn T, Zibek S, Gagliardini A, et al (2022) Characterization of chitin and chitosan derived from Hermetia illucens, a further step in a circular economy process. *Sci Rep* **12**, 6613.
28. Muthu MS, Xavier SSJ, Ajith P, Anand DP (2022) Preparation and characterization studies of nano graphene oxide. *Mater Today Proc* **66**, 2449.
29. Esmaeili Y, Bidram E, Zarrabi A, Amini A, Cheng C (2020) Graphene oxide and its derivatives as promising *in vitro* bio-imaging platforms. *Sci Rep* **10**, 18052.
30. Zaboon MH, Saleh AA, Al-Lami HS (2019) Comparative cytotoxicity and genotoxicity assessments of chitosan amino acid derivative nanoparticles toward human breast cancer cell lines. *Egypt J Chem* **62**, 2061.
31. Ali S, Dayo M, Alahmadi S, Mohamed A (2024) Chitosan-supported ZnO nanoparticles: their green synthesis, characterization, and application for the removal of pyridoxine HCl (vitamin B6) from aqueous media. *Molecules* **29**, 828–842.
32. Sowjanya B, Sirisha U, Juttuka AS, Matila S, King P, Vangalapati M (2022) Synthesis and characterization of zinc oxide nanoparticles: Its application for the removal of alizarin red S dye. *Mater Today Proc* **62**, 3968.
33. Bashal AH, Riyadh SM, Alharbi W, Alharbi KH, Farghaly TA, Khalil KD (2022) Bio-based (chitosan-ZnO) nanocomposite: synthesis, characterization, and its use as recyclable, eco-friendly biocatalyst for synthesis of

thiazoles tethered azo groups. *Polymers* **14**, 386.
34. Zhang J, Bai J, Duan M, Yang J, Bian L (2021) Derivation of adsorption capacity and adsorption isotherm by a single adsorbate concentration in liquid-solid system. *Chem Pap* **75**, 2459.
35. Li S, Huang L, Zhang H, Huang Z, Jia Q, Zhang S (2021) Adsorption mechanism of methylene blue on oxygen-containing functional groups modified graphitic carbon spheres: Experiment and DFT study. *Appl Surf Sci* **540**, 148386.
36. Kanwal S, Devi P, Ahmed Z, Qambrani NA (2024) Adsorption isotherm, kinetic, and thermodynamic studies for the adsorption of fluoride on waste marble powder. *Desal Water Treat* **319**, 100441.
37. Ortiz AV, Lopez KJF, Toro RO (2022) Kinetics and adsorption equilibrium in the removal of azo-anionic dyes by modified cellulose. *Sustainability* **14**, 3640.
38. Hajyani Z, Mousavi Z, Soleimanbeigi M, Wong YJ (2025) Antibiotic adsorption from real pharmaceutical factory wastewater using a hole-punched flat ceramic membrane based on clay and hydroxyapatite in a fixed bed module. *Results Eng* **26**, 105364.
39. Tichem TM, Wang Y, Gameli RBH, Mbage B (2023) Multicomponent adsorption of pollutants from wastewater using low-cost eco-friendly iron-modified rice husk biochar in the era of green chemistry. *Sustainability* **15**, 16348.
40. Molleda YFC, Barboza NMC, Mina SP, Valcarcel CED, Malpartida YGP, Redolfo RL, Quisani AM, Florez MC, et al (2025) A study of methylene blue adsorption by a synergistic adsorbent algae (*Nostoc sphaericum*)/activated clay. *Polymers* **17**, 2134.
41. Chen Z, Sheng J, Ren K, Song Y (2026) Low-cost, high-stability aerogel for methylene blue dye adsorption. *Int J Environ Anal Chem* **106**, 585–602.
42. Gunes B, Jaquet Y, Sánchez L, Pumarino R, Mcglade D, Quilty B, Morrissey A, Gholamvand Z, et al (2021) Activated graphene oxide-calcium alginate beads for the adsorption of methylene blue and pharmaceuticals. *Materials* **14**, 6343.
43. Seth S, McGillivray M (2018) Composite indices, alternative weights, and comparison robustness. *Soc Choice Welf* **51**, 657.
44. Chen X, Hossain Md F, Duan C, Lu J, Tsang YF, Islam MdS, Zhou Y (2022) Isotherm models for adsorption of heavy metals from water: A review. *Chemosphere* **307**, 135545.